Detailed studies of mid-ocean ridge volcanism at the Mid-Atlantic Ridge (45N) and elsewhere

YEO, ISOBEL,ALICE,L

Earth and Planetary Science Letters 299 (2010) 228–241

Contents lists available at ScienceDirect

Earth and Planetary Science Letters

journal homepage: www.elsevier.com/locate/epsl

Structure and development of an axial volcanic ridge: Mid-Atlantic Ridge, 45°N

R.C. Searle [a,*], B.J. Murton [b], K. Achenbach [a], T. LeBas [b], M. Tivey [c], I. Yeo [a], M.H. Cormier [d], J. Carlut [e], P. Ferreira [f], C. Mallows [a], K. Morris [b], N. Schroth [b], P. van Calsteren [g], C. Waters [c,1]

[a] Department of Earth Sciences, Durham University, Durham DH1 3LE, UK
[b] National Oceanography Centre, Empress Dock, Southampton SO14 3ZH, UK
[c] Department of Geology and Geophysics, Woods Hole Oceanographic Institution, Woods Hole, MA 02543, USA
[d] Department of Geological Sciences, University of Missouri, Columbia, MO 65211-1380, USA
[e] UMR 8538, Ecole Normale Supérieure, 24 Rue Lhomond, 75231 Paris CEDEX 5, France
[f] Instituto Nacional de Engenharia, Tecnologia e Inovação, Lisbon, Portugal
[g] Department of Earth Sciences, Open University, Milton Keynes MK7 6BJ, UK

ARTICLE INFO

Article history:
Received 18 March 2010
Received in revised form 31 August 2010
Accepted 1 September 2010
Available online 29 September 2010

Editor: M.L. Delaney

Keywords:
axial volcanic ridge
Mid-Atlantic Ridge
oceanic spreading centre
seafloor spreading
seafloor volcanism

ABSTRACT

We describe the most comprehensive and detailed high resolution survey of an axial volcanic ridge (AVR) ever conducted, at 45°N on the Mid-Atlantic Ridge. We use 3 m resolution sidescan sonar, deep-towed magnetic field measurements, video observations from eleven ROV dives, and two very-high-resolution bathymetry and magnetic surveys. The most recently active AVR has high topographic relief, high acoustic backscatter, high crustal magnetization and little faulting. It is sharp-crested, 25×4 km in extent and 500 m high, and is covered by approximately 8000 volcanic "hummocks" whose detailed nature is revealed for the first time. Each is an individual volcano ≤450 m in diameter and ≤200 m high, ranging from steep-sided (45°) cones to low domes. Many have suffered significant flank collapse. Hummocks tend to align in rows parallel to the AVR axis, parallel to its NE-trending spurs or, on its lower flanks, sub-normal to the AVR trend. These latter are spaced 1–2 km apart and comprise 1–2 km-long rows of single volcanoes. We infer that their emplacement is controlled by down-flank magma transport, possibly via lava tubes. The AVR contains only one large flat-topped seamount. The flanking median valley floor consists of either older hummocky volcanic terrain or flat-lying, mostly sediment-covered lavas. These typically have low-relief lobate surfaces, inflation and collapse structures, and occasional lava tubes and tumuli. The AVR displays open fissures, mostly along its crest. There is direct evidence for only a few small faults on the AVR, though steep, outward-facing slopes draped by elongate pillows may be small normal faults covered by lava. The surrounding median valley floor is heavily fissured. Normal faults cut it and an older AVR, the latter displaying significant outward facing faults. High crustal magnetization, an approximate proxy for crustal age within the Brunhes, is confined to the active AVR. Magnetic palaeointensity measurements are consistent with ages up to ~12 ka for several samples from the active AVR and ≥12 ka for one sample from the median valley floor. This is much less than the predicted spreading age, implying distribution of melt off-axis or episodic AVR growth.

1. Introduction

Axial volcanic ridges (AVRs) have been recognised in most Mid-Atlantic Ridge (MAR) spreading segments (Ballard and Van Andel, 1977; Bellaiche et al., 1974; Bideau et al., 1998; Briais et al., 2000; Brown and Karson, 1989; Bryan et al., 1994; Gente et al., 1991; Gracia et al., 1998; Karson et al., 1987; Kong et al., 1988/89; Lawson et al., 1996; Parson et al., 1993; Sempéré et al., 1990; Smith and Cann, 1992). They are tens of kilometres long, a few kilometres wide and a few hundred metres high, comprising agglomerations of small volcanic "hummocks". However, there have been few comprehensive studies using detailed high resolution surveys across whole AVRs.

Because AVRs are formed entirely within the Brunhes chron (<780 ka), their formation and growth have not been dated; importantly, it is unclear whether they are episodic or steady state. At MAR 37°N, Ballard and Van Andel (1977) estimated a volcanic cycle of 180 kyr based on ages interpolated from the last magnetic reversal, while Bryan and Moore (1977) estimated a lifespan of 10 kyr for a single volcanic complex using manganese crust thickness. At MAR 25°N, Cann and Smith (2005) used sediment thickness to estimate age, inferring continuous eruption of smooth and hummocky lava

* Corresponding author. Tel.: +44 191 334 2307; fax: +44 191 334 2301.
E-mail addresses: r.c.searle@durham.ac.uk (R.C. Searle), bjm@noc.soton.ac.uk (B.J. Murton), mtivey@whoi.edu (M. Tivey), cormierm@missouri.edu (M.H. Cormier), jcarlut@mailhost.geologie.ens.fr (J. Carlut), pedro.ferreira@ineti.pt (P. Ferreira), P.V.Calsteren@open.ac.uk (P. van Calsteren).
[1] Now at: Department of Geology and Geophysics, Dept. 3006, 1000 University Ave., University of Wyoming, Laramie, WY 82071, USA.

0012-821X/$ – see front matter © 2010 Elsevier B.V. All rights reserved.
doi:10.1016/j.epsl.2010.09.003

flows in different parts of the segment over 250 kyr. New AVRs are estimated to form on the MAR every 25 kyr (Ballard and Van Andel, 1977; Barclay et al., 1998) to 600 kyr (Searle et al., 1998b; Thatcher and Hill, 1995), and on the ultra-slow spreading Southwest Indian Ridge from 0.4 Myr to 2.4 Myr (Mendel et al., 2003). Sinha et al. (1998) estimated that a sub-AVR melt lens on the southern Reykjanes Ridge represented 20 kyr of crustal growth but would freeze after 1.5 kyr. Sturm et al. (2000) inferred an AVR age ~10 ka at MAR 23°N using U-series decay. Such young ages are much less than crustal age implied by average spreading rate, implying highly episodic volcanism. Qualitative life cycles, based on comparison of several AVRs assumed to be at different stages of development, have been proposed by Mendel et al. (2003) and Parson et al. (1993) but are largely untested.

We report the most comprehensive and detailed high resolution survey of a complete AVR yet conducted, as part of a larger project that aims to date development of the MAR 45°N AVR using U-series methods. We use detailed imaging and magnetic measurements to develop a geological map of the AVR and surrounding seafloor and to make preliminary estimates of age relations. We clearly identify for the first time the nature of the ubiquitous volcanic "hummocks" as small single volcanoes, and find that many suffer significant flank collapse. An important component of the AVR is short spurs normal to its overall trend composed of lines of these hummocks. We identify flat-lying smooth lava flows flanking the AVR, and show that tectonic strain develops progressively across the AVR and median valley floor. We map areas of inferred youngest crust using magnetic intensity as a proxy for age, and directly infer some ages from magnetic palaeointensity measurements. We find that AVR volcanism is of restricted age and relatively young, compatible with highly episodic development. Detailed chemical and petrological analyses and uranium-series dating will be reported elsewhere.

This region was extensively studied in the 1960s and 1970s (Aumento et al., 1971). A multibeam bathymetry survey was conducted in 1990 and extended in 1993 (Keeton and Searle, 1996; Mello et al., 1999). This showed a well-defined AVR within a typical "hour glass" median valley with small, dextral, non-transform offsets to north and south. Those limited resolution data showed that the AVR contains a wide variety of volcanic morphologies, including linear ridges, hummocky volcanoes, flat-topped seamounts, and possibly lava terraces (Smith and Cann, 1999). The region has a very high geochemical diversity (Mello et al., 1999), which we judged might facilitate geochemical fingerprinting of different melt batches.

2. Data acquisition

We first conducted a sidescan sonar and magnetic field survey using the deep-towed instrument TOBI (Flewellen et al., 1993), comprising two N–S tracks and twenty-two E–W lines spaced 1.4 km apart, and concurrently collected multibeam bathymetry (Fig. 1). We then made 13 dives with the remotely operated vehicle (ROV) *Isis* (German et al., 2003).

2.1. Multibeam bathymetry

Multibeam bathymetry was acquired using a ship-mounted Simrad EM-120 echosounder with GPS navigational precision of 10 m. The slow survey speed and closely-spaced tracks produced significant oversampling, letting us grid the data at 50 m resolution (Fig. 1). Initial processing was carried out using CARIS HIPS version 6.1 software, with final display utilising GMT (Wessel and Smith, 1998).

2.2. TOBI

TOBI's instrumentation included a 30 kHz sidescan sonar and three-component magnetometer. The survey produced sidescan mosaics with 100% coverage (no gaps or degraded nadir sections visible) in both north- and south-looking directions (Fig. 2), together with east- and west-looking mosaics with some gaps. See Supplementary material for details of sonar processing. Three-component magnetic field data were corrected for the magnetization of the TOBI vehicle and inverted for crustal magnetization assuming a constant 0.5 km thick source layer that follows the seafloor topography, using standard methods (Guspi, 1987; Isezaki, 1986; Korenaga, 1995; Parker and Huestis, 1974). Because our entire magnetic survey lies within the Brunhes normal magnetisation zone, we added 14 times the annihilator (Parker and Huestis, 1974) to make the inferred magnetization everywhere positive (Fig. 3; see Supplementary material for details).

2.3. ROV Isis

Isis carried a number of video and still cameras, and was navigated by a combination of Sonardyne ultra-short-baseline acoustic fixes and 300 kHz Doppler sonar. Eleven of our *Isis* dives were used for continuous video surveillance and sampling, and provide extensive ground truthing for the sonar interpretation.

The other two dives provided detailed, high-resolution topographic and magnetic surveys: dive 91 covered a 2.5 km square over the eastern flank of the AVR near 45°29′N (Fig. 4), while dive 87 covered a 0.8 km-wide oblique strip across the AVR and median valley floor near 45°35′N (Supplementary Fig. 2). Both surveys were flown approximately 100 m above the seafloor with 180 m spaced tracks yielding almost 100% topographic coverage. Topography was measured using the ultra-high-resolution MS2000 multibeam echosounder, with data gridded to 0.5 m resolution (Fig. 4a, Supplementary Fig. 2a). Magnetic field was measured on a three-component magnetometer, then processed in a similar manner to the TOBI magnetic data, with the addition of nine times the annihilator for dive 91 (Fig. 4b, Supplementary Fig. 3) and fifteen times for dive 87 (Supplementary Fig. 2).

3. Results

3.1. Topography

The width of the 45°N segment floor ranges from 5 km at its centre to 8 km in the south and 12 km in the north (Fig. 1), with short (5 km and 3 km) dextral non-transform offsets (NTOs) to north and south.

The main AVR runs 18 km from 45°24′N to 45°35′N, with a sharp, linear crest and monotonically deepening flanks. Although the topographic ridge extends a further 11 km north to about 45°41′N, this northern part has a less well-defined crest and rougher flanks. Both bathymetry and sidescan show the main AVR is largely devoid of faulting, whereas the northern extension is significantly broken up by N–S trending fault scarps, especially north of 45°36′N. The main AVR is roughly bounded by the 3000 m isobath. For most of its length its crest is shallower than 2700 m and reaches up to 500 m above the median valley floor. By contrast, the northern extension is mostly deeper than 2900 m.

The crest of the main AVR trends 006°, close to the 007.9° normal to the predicted spreading direction (DeMets et al., 1994) and to the overall trend of this segment. It is placed somewhat asymmetrically within the median valley floor, abutting the first valley wall fault to the east, but having a 2–3 km-wide area of fairly flat valley floor between it and the first major fault to the west.

Within the AVR are many narrow ridges, which the sidescan data show to be composed of lines of volcanic hummocks. While most are parallel to the overall AVR trend, at 45°30′N they fan out to form a prominent, oblique, NNE trending spur (*a*, Fig. 1). Smaller oblique spurs occur near 45°29′N and 45°35′N on the east flank and near 45°25′N in the SW (e.g., *b*, Fig. 1). Many small spurs also occur, more or less orthogonal to the main AVR trend (e.g. *c*–*e* and lower inset,

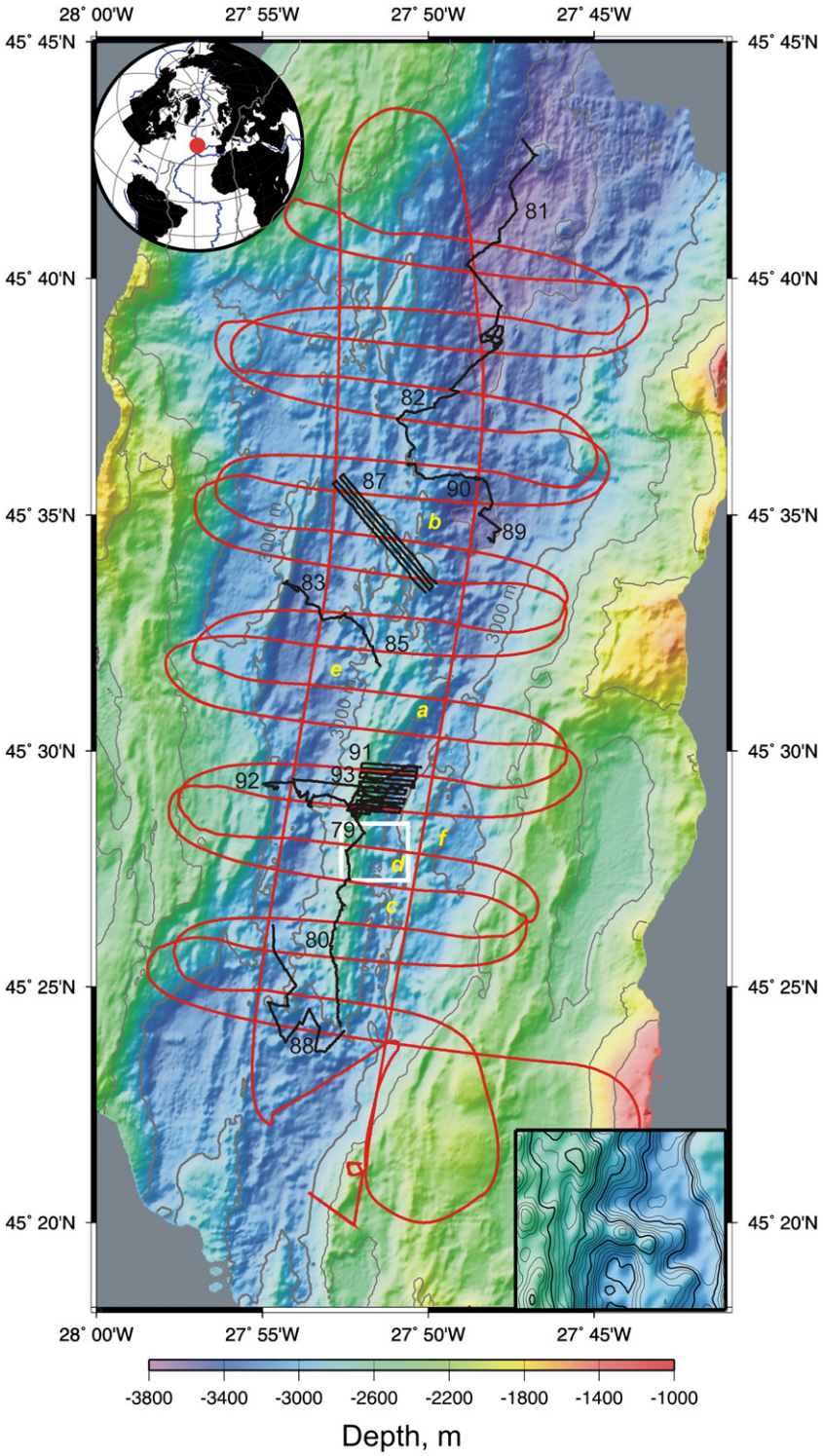

Fig. 1. Shaded bathymetry of the study area, with TOBI tracks (red) and *Isis* tracks and dive numbers (black). Depth contours (grey) are shown at 400 m intervals; 3000 m contour is bold. Illumination from NW. Top left inset shows location. Bottom right inset shows detail of bathymetry in region of white rectangle. See Section 2.1 for processing details. Yellow letters identify features discussed in the text.

Fig. 1). The sidescan data reveal that they consist of rows of up to about six aligned volcanic hummocks (inset, Fig. 2).

The detailed bathymetry from dive 91 shows that this ~4 km^2 area covering the eastern flank at the centre of the AVR contains some 100 volcanic hummocks. They have heights up to 200 m, diameters from 20 to 450 m, and steep flanks sloping 40° ± 20° (Fig. 4a; Yeo et al., under revision). Approximately half of these have partially collapsed (e.g., *1*, Fig. 4a). Lines of hummocks run along the AVR crest (*2*), parallel to but below the crest (*3*), some follow an arc curving from mid-flank towards the NE to form an oblique spur (*4*), while some extend at right angles to the AVR crest (*5*). There are several N–S fissures, including a prominent one along the AVR crest (*6*). Small outward-facing faults below the AVR crest define a small axial horst (*7*, *8*). Several localised scarps are associated with volcano collapse

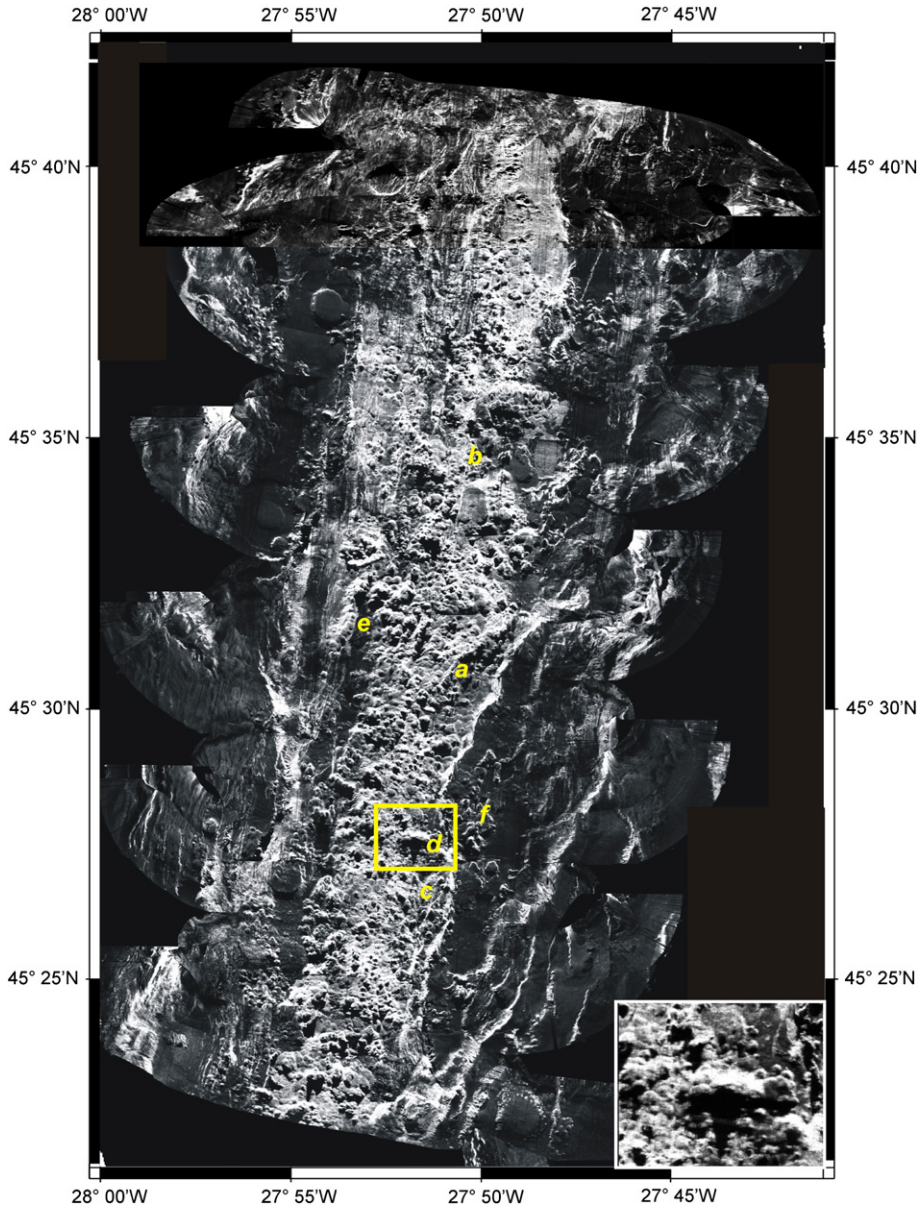

Fig. 2. TOBI sidescan sonar mosaic, with light tones indicating high acoustic backscatter. Insonification is from the north except north of 45°38′N where it is from the south. Inset shows detail from same area as inset on Figure 1, outlined by yellow rectangle. See Section 2.2 for processing details.

(Yeo et al., under revision). The high-resolution bathymetric survey from dive 87 showed similar features and is described in the Supplementary material.

3.2. Magnetization

Crustal magnetization inferred from TOBI data shows an elongated magnetization high — the central anomaly magnetic high (CAMH; Klitgord, 1976; Tivey and Johnson, 1987) centred over the main AVR (Fig. 3). The magnetization peaks over the AVR crest, exceeding 22 A m^{-1} over the entire length of the main AVR, with maxima (>26 A m^{-1}) at 45°24.5′N and 45°31.2′N. It falls in a steep gradient about 4 km east and west of the AVR crest to the flanking median valley floor, making the CAMH about 8 km wide. North of the main AVR the CAMH flanks become less steep and it peaks at <20 A m^{-1}.

The high-resolution magnetization maps from the *Isis* dives reveal significantly more detail. The dive 91 area reveals a pair of narrow, 18–20 A m^{-1} ridges about 150 m either side of the AVR crest, with a narrow, discontinuous magnetization trough of 6–10 A m^{-1} in between (Fig. 4b). Significantly, there is a parallel and more continuous N–S trending magnetization high 600 m E of the AVR crest, peaking at 16 A m^{-1}. This high follows a line of volcanic hummocks marking a bathymetric bench; it then curves to follow the oblique, NE-trending topographic spur, where it divides into two circular highs of 14 and >16 A m^{-1}. A further broad region of slightly elevated magnetization occurs at the eastern edge of the survey. All these patterns are robust to different amounts of added annihilator (Supplementary Fig. 3). The dive 87 magnetization map (Supplementary Fig. 2b, d) also shows magnetization peaks up to 24 A m^{-1} over the ridge crest and the flanking lines of cones, with very low magnetizations in between. In both areas, the amplitude of magnetization is more variable and patchy than is predicted by simple models of field reversal and decay at a uniform spreading rate (e.g., Allerton et al., 2000).

3.3. Sonar interpretation

In interpreting the sidescan sonar data we follow similar principles to previous authors (Blondel and Murton, 1997; Briais et al., 2000;

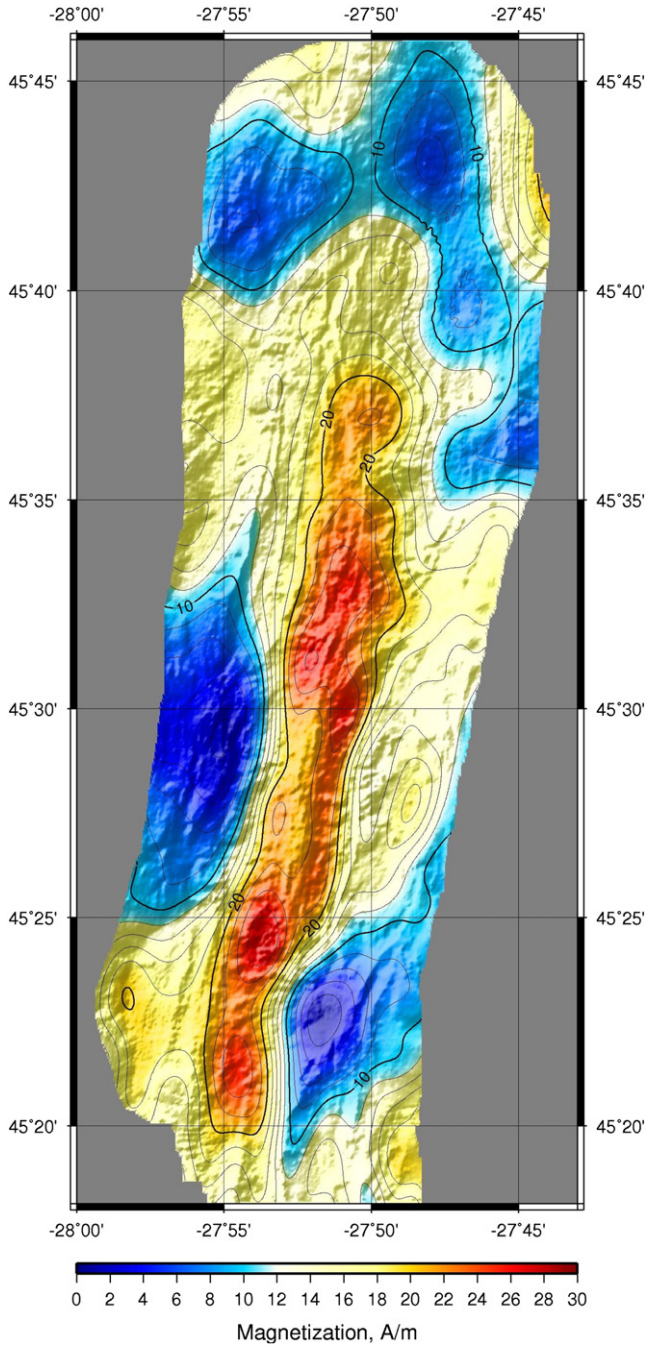

Fig. 3. Crustal magnetization deduced by inversion of the TOBI magnetic field, draped over shaded bathymetry. Fourteen times the annihilator has been added to make the solution everywhere positive. Contour interval 2 A m^{-1}. Bathymetry illuminated from the NW. See Supplementary materials for details of magnetic processing.

Cann and Smith, 2005; Gracia et al., 1998; Head et al., 1996; Lawson et al., 1996; Parson et al., 1993; Sauter et al., 2002; Searle and Bralee, 2007; Smith et al., 1995) to divide the sonar images into a number of different acoustic terrains. We follow the distinction introduced by Cann and Smith (2005) of separate terminology for a) lava morphologies observed visually and divided into sheet flows, lobate and pillow lavas, as against b) volcanic terrains observed by sonar and divided into hummocky and smooth flows or terrains. We give details of our interpretations in Table 1, with examples of their acoustic signals in Fig. 5. We used the *Isis* video data (e.g., Fig. 6) to ground-truth our sonar interpretations, then compiled the latter into a geological map of the study area (Fig. 7).

4. Geology of the ridge axis

4.1. Hummocky volcanic terrain

The main AVR corresponds closely to the distribution of recent hummocky volcanoes. The comparison of TOBI sidescan sonar with high-resolution bathymetry and video data from dive 91 (Yeo et al., under review) confirms, for the first time, that each individual TOBI reflector corresponds to a small domed or conical volcano. *Isis* videos show they are composed mostly of pillow lavas, elongated pillows (especially where draped over steep slopes), and pillow breccias (Fig. 6, a–d), with some lobate pillows. Many are topped by a small "haystack" composed of steeply draped pillows and jumbled lava (Fig. 6e). Many of the volcanoes have undergone some degree of sector collapse, and in these cases truncated pillows are seen in the collapse scars and talus at their bases, as well as in linear fault scarps (Fig. 6f).

The young hummocky terrain is partially surrounded by "older hummocky volcanoes". The boundary between them can be abrupt on the east and west flanks of the AVR, but is often gradational going from the main AVR to its northern extension, perhaps reflecting the difficulty for dykes to intrude off-axis into lithosphere of rapidly increasing strength and thickness, compared to relatively easy along-axis propagation into very young, weak lithosphere.

We attempted to estimate relative ages of pillow lavas using their visual appearance and sediment cover (Cann and Smith, 2005; Lawson et al., 1996; Sturm et al., 2000), but no coherent pattern was apparent. Throughout the area of recent and older hummocky volcanoes, *Isis* video and photographic coverage show pillows with sediment cover ranging from a light dusting (Fig. 6a) to several millimetres with pockets of several centimetres or more between pillows (Fig. 6b). We observed a common pattern of fairly extensive sediment cover on flat-lying areas at the bases of volcanoes, decreasing sediment cover with increasing height on their flanks, and nearly bare summits. This is repeated on many unrelated volcanoes over different parts of the AVR. We judge it unlikely that all these represent coeval, recent eruptions, and conclude that the sediment pattern is controlled more by volcano morphology than by age. This confirms the findings of (Sturm et al., 2000) that visual appearance and sediment cover are not reliable indicators of young lava age. However, the change in sonar texture, together with the reduced magnetization and increased incidence of faulting in the north, suggest that the northern volcanic ridge is indeed older than the main AVR. Recent hummocky volcanoes extend south of the topographically defined AVR at least as far as 45°22.5′N. This is also a region of continued high magnetization (Fig. 3), suggesting very recent volcanism here.

The east flank of the main AVR with its young volcanic terrain abuts the first valley-wall fault to the east. On the terrace above this fault is a small area of older volcanic terrain (*f*, Fig. 1). It appears distinctly older based on the sonar imagery, so is not an up-faulted part of the current AVR and is inferred to be part of an older AVR that has been split. It is flanked to the east by completely sedimented seafloor. The northeast and southwest sides of the main AVR are flanked by older hummocky volcanoes, which in turn are flanked on their distal sides by very old and/or heavily sedimented volcanic seafloor extending to the first valley wall faults. The terraces above these faults are characterised by very old hummocky lavas or complete sediment cover. The older, northern extension of the AVR is flanked to both east and west by very old and/or heavily sedimented volcanic terrain.

Other outcrops of older hummocky seafloor occur patchily in the floor of the median valley and in the median valley walls. Their acoustic appearance suggests they are parts of older, defunct, partially dismembered and partially buried AVRs.

4.2. Smooth volcanic terrain

The apparently youngest smooth flows occur in the northern NTO basin and immediately east of the main AVR, and were extensively

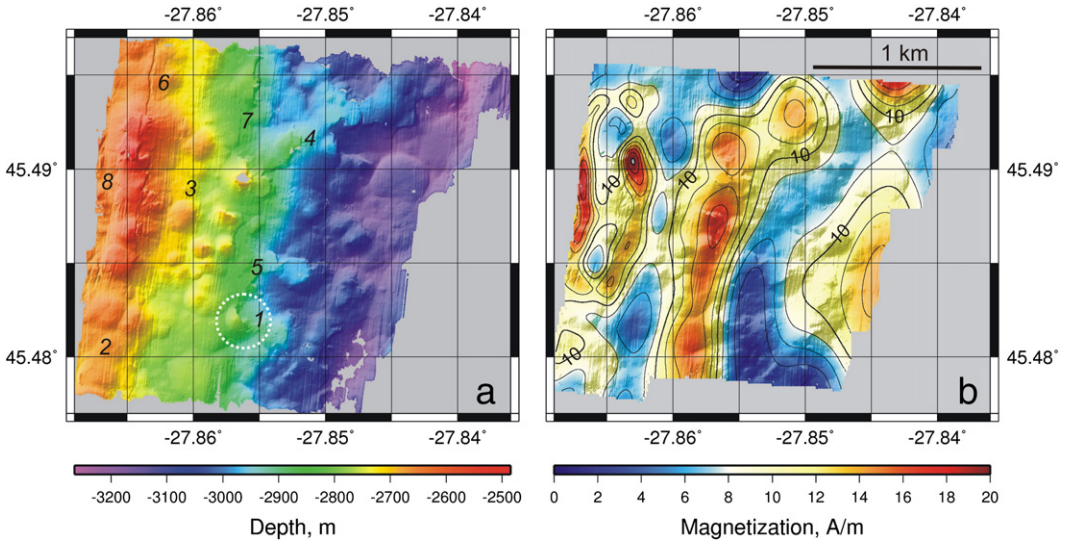

Fig. 4. (a) High resolution bathymetry, illuminated from NW, and (b) crustal magnetization (contour interval 2 A m^{-1}) draped over shaded bathymetry, from dive 91 over the eastern flank of the AVR. Nine times the annihilator has been added to the magnetisation to make the solution everywhere positive. Coverage extends from the AVR crest (~27.865°W) in the west to the foot of the first valley-wall fault in the east. See Section 2.3 for details of data acquisition and processing. White circle outlines a volcano showing prominent flank collapse (see Section 4.1). Black numerals identify features discussed in the text.

examined by dives 81, 82 and 89. *Isis* video shows extensive but thin (<20 cm) sediment cover, with occasional outcrops of tumuli, flattened pillows or lobate flows but no evidence of bulbous pillows or volcanic cones (Fig. 6g). Pahoehoe is seen occasionally (Fig. 6i) but is very rare. Open lava tubes are occasionally seen, where exposed in fault scarps (Fig. 6h). One feeder dyke was observed in a small fault scarp (Fig. 6j).

Areas mapped as older smooth flows (Fig. 7) all lie in the median valley floor west of the AVR, abutting both young and older hummocks and confirmed by dives 83, 88, and 92. They are covered by tens of centimetres to a metre or more of sediment, often partly indurated (Fig. 6k). We do not see acoustic "smooth flows" in the median valley walls, but any such flows there would likely be masked by sediment.

4.3. Seamounts

Nineteen flat-topped and mostly circular seamounts are recognised (Fig. 7). Only one is clearly part of the AVR, sitting high on its eastern flank at 45°34′N, 27°50′W, under the SE corner of the dive 87 survey (Supplementary Fig. 2a). It must be of similar age to or younger than the AVR. It is markedly non-circular, and may be a lava terrace (Smith and Cann, 1999).

Three other seamounts abut the recent lavas of the AVR at the feet of its northeast and southwest flanks; we cannot determine their relative ages with respect to the AVR. The rest of the seamounts are in the rift valley walls or northern NTO, and generally have low-backscatter tops (Fig. 2) indicating significant sediment cover and therefore age.

4.4. Faulting

The main AVR is devoid of major faulting. East- and west-looking sidescan images show small outward facing faults just west of the AVR crest near 45°29′N and a small inward facing fault on the E flank between 45°26′N and 45°28′N (Fig. 7). Small offset (~5 m) outward-facing faults define a small horst at the AVR crest (*8*, Fig. 4a), and a small outward facing fault occurs on its west flank at 45.585°N, 27.864°W (Supplementary Fig. 2a). Some features mapped as axis-parallel volcanic lineaments may consist of lavas draped over small fault scarps, and might even be "volcanic growth faults" (Macdonald et al., 1996). In contrast, the older AVR north of 45°35′N displays several large, mostly outward-facing faults on its W flank (45°35′N–45°40′N, 27°50′W–27°52′W; Fig. 7).

Small-scale faulting or fissuring is common on the median valley floor to the west of the AVR, clearly visible on sidescan images and confirmed especially by *Isis* dive 83 (Fig. 6k,l). Similar features extend across the northern, older AVR and into the NTO. The only faulting or fissuring between the east flank of the AVR and the first valley-wall fault is over the young smooth flows (dives 81, 82 and 89), where minor faulting allowed us glimpses of the volcanic basement below the sediments (e.g. Fig. 6g).

Near the segment centre at 45°27′N, the first major faults, with throws of hundreds of metres, begin 1.8 km east and 3 km west of the AVR crest; towards the ends of the AVR, the first major faulting occurs around 4 km and rarely 8 km from the axis.

4.5. Sediments

We observed semi-indurated sediments up to ~1 m thick at the tops of fissures in areas of old, smooth lavas on the median valley floor (Fig. 6k). Except for the northern NTO, areas mapped from sidescan as having complete sediment cover are confined to the rift valley walls. We infer the sediment cover there to be >1 m thick.

5. Palaeointensity dating

Previous studies document the feasibility of magnetic palaeointensity dating for mid ocean ridges samples (Bowles et al., 2006; Carlut and Kent, 2000; Carlut et al., 2004; Gee et al., 2000). In an initial attempt to constrain the age of the AVR and its components, we measured magnetic palaeointensities on 30 sub-samples of basaltic glass.

All the palaeointensity experiments were carried out at the palaeomagnetic laboratory of l'Institut de Physique du Globe, Paris, using a 2G cryogenic magnetometer and the modified Thellier and Thellier method (Coe, 1967; Thellier and Thellier, 1959). Small glassy fragments weighing 300–1100 mg were put into 1×3 cm Pyrex-glass tubes and retained with glass microfiber paper. All infield experiments were performed in air in an applied field of 30 μT. Samples were heated to 120 °C then at 40 °C intervals until less than 20% of natural magnetization was left (usually at ~400 °C). Possible thermal

Table 1
Geological and acoustic terrains.

Name	Acoustic character	Interpretation	Comments	Sonar example	Photo example
Recent hummocky volcanoes	Small (~50–500 m diameter) arcuate to sub-circular high intensity reflections and associated deep shadows, named "hummocks" by previous authors. Heights up to 200 m and variable height/diameter ratio.	Each curved reflection or shadow corresponds to a single volcanic cone built of pillows, lobate and elongated pillows, with minimal sediment cover.	Interpretation based on comparison with the high-resolution bathymetry and video data from *Isis* dives, e.g. dive 91 (Yeo et al., under revision).	Figure 5a	Figure 6a–e
Older hummocky volcanoes	Very similar to recent hummocks, but with lower acoustic contrast and fewer very-high- or very-low-intensity areas.	Hummocky volcanoes with modest (tens of cm) sediment cover; inferred to be older than recent hummocky volcanoes	Contacts with recent or very old hummocky volcanoes may be sharp or gradual.	Figure 5b	
Very old hummocky volcanoes	Similar to older hummocky terrain, but with overall much lower backscatter and only isolated high reflectivity areas indicating sparse outcrops of lava.	Hummocky volcanoes overlain by significant (~>1 m) sediment cover.		Figure 5c	
Seamounts	Bright arcuate reflector facing sonar and/or arcuate shadow facing away. Central circular region of uniform backscatter, bright to dark depending on age, possibly with one or more craters.	Flat-topped, steep-walled, circular seamounts with diameters of 500 m–1200 m and height to diameter ratios ~0.1.	Distinguished from hummocky volcanic cones by being much larger with broad, flat or slightly domed summits, rather than sharp peaks.	Figure 5d	
Younger smooth flows	Relatively uniform, slightly mottled, mid-level backscatter and very low bathymetric slopes.	Low relief, mostly lobate lavas; almost entirely covered by thin (<~1 m) sediments.	Interpretation confirmed by *Isis* dives 81–82, and 89.	Figure 5e	Figure 6g–i
Older smooth flows	Very low backscatter with occasional small high backscatter areas, and very low bathymetric slopes.	Low relief lava flows that have been almost completely buried by several metres of sediment.	Confirmed by *Isis* dives 83, 88 and 92. Where revealed by faulting, features are similar to those in younger smooth flows.	Figure 5f	Figure 6k
Other old outcrops	Moderate bathymetric relief with very low acoustic backscatter, with a few areas of high backscatter.	Extensive sediment with occasional outcrops of unidentifiable rock.	Indistinct acoustic patterns with appreciable sediment hide geological nature of the terrain.	Figure 5g	
Volcanic lineaments	Small bathymetric ridges with moderate slope; usually less steep, less linear and less extensive than fault scarps. On sidescan, narrow lines of hummocks.	Lines of volcanic cones, usually only one cone wide.	Inferred to lie above eruptive fissures.	Figure 5h	
Sediment	Fairly uniform low backscatter regions with no high backscatter areas.	100% sediment cover. Subtle mottling sometimes suggests underlying volcanic terrain.	Distinguished from acoustic shadow by low residual backscatter.	Figure 5i	
Faults	Extensive, linear, narrow areas of high backscatter, usually associated with steep (≥30°) bathymetric slopes.	Dip-slip faults with vertical offsets>~10 m.	Older or larger-offset faults often display gullying and/or basal talus fans.	Figure 5j	
Small faults and fissures	Very narrow bands of linear high or low backscatter that cut across other terrains.	Small faults and fissures with vertical offsets<~10 m.	Unresolved by ship-based bathymetry.	Figure 5d, k	Figure 6k,l

alteration of samples was monitored by performing a pTRM check after alternate temperature steps. To be accepted, a sample had to show positive pTRM checks, i.e. lie within 5% of the initial pTRM values. It also had to show a single component of magnetization and a linear relation between lost and acquired magnetization over a few steps. Many samples gave negative pTRM checks. Most samples gave a magnetization near or only slightly above experimental noise level (~10^{-11} A m^2), and only seven, with magnetization >5×10^{-9} A m^2, passed our selection criteria (Carlut et al., 2004) and were deemed suitable for further analysis. A typical example of a successful Thellier experimental result is shown in Supplementary Fig. 4.

Measured palaeointensities range from 28 μT to 68 μT. They were converted to virtual axial dipole moments (VADM; Table 2). Only one sample could be measured for each unit, but as previously observed (Carlut and Kent, 2000; Carlut et al., 2004; Mejia et al., 1996; Pick and Tauxe, 1993), the expected dispersion is low. An uncertainty of 0.7×10^{22} A m^2 was given to all the results, corresponding to twice the mean standard error from all individual units published by Carlut et al. (2004) on the same kind of material.

The resulting VADMs were compared with a compilation of measured VADM against time (Knudsen et al., 2008; Fig. 8). To reduce age ambiguity, we assume the samples are younger than about 50 ka, when the Earth's field was last as strong as at present (Guyodo et al., 1999). Recent sedimentation rates at 45°N have exceeded a few centimetres per thousand years (Keen and Manchester, 1970), so 50 ka seafloor should have accumulated >50 cm of sediment, which we do not see on the AVR except in very localised basins.

The measured samples gave sensible results except for sample 93-38 from the AVR crest, which returned a VADM of 21.5×10^{22} Am^2; this is twice as high as any recent geomagnetic field strength. This sample had the lowest NRM (5.7×10^{-9} A m^2) which might indicate experimental limitation at a higher threshold than expected. It was discarded as erroneous. Two samples from the lower east flank of the AVR (79-10 and 79-13) gave the next highest VADMs, values only exceeded in the comparison curve for fields ~3 ka age, but also close to the value at 9 ka, which we take to be a maximum age. We thus infer ages for samples 79-13 and 79-10 of 1–4 ka or ~9 ka. Samples 79-11 (also from the lower east flank of the AVR) and 92-24 (mid-way down

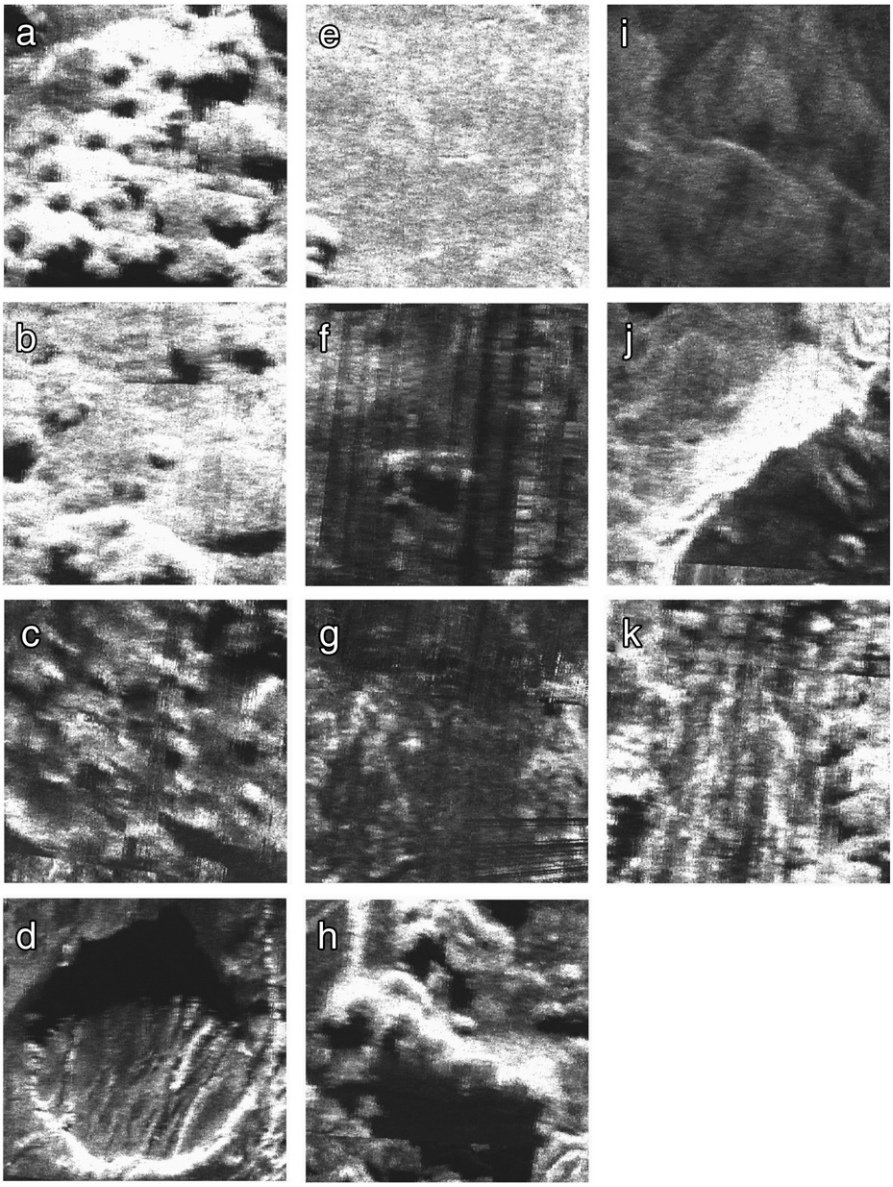

Fig. 5. Acoustic terrains observed in TOBI sidescan sonar data. Panels were extracted from Figure 2 with no further processing, so relative amplitudes and contrasts reflect actual terrains. Each panel is 1 km^2. These terrains are discussed in Section 3.3. a) "Recent hummocky volcanoes"; b) "older hummocky volcanoes"; c) "very old hummocky volcanoes"; d) "seamounts"; e) "young smooth lava flows"; f) "older smooth lava flows"; g) "other old outcrops"; h) "volcanic lineaments"; i) "sediment"; j) "faults"; k) "small faults and fissures".

the west AVR flank) gave palaeointensities suggesting ages most likely <12 ka. Sample 79-3 is from the very base of the AVR adjacent to the first valley wall fault; its palaeointensity suggests an age anywhere in the 5 ka–40 ka range. Sample 92-8, from the median valley floor, yields the lowest palaeointensity and the oldest age range of 12 ka–50 ka.

These results and their interpretation should be taken with caution at this stage and need confirmation, but they provide a first estimate for the age range of the tested samples. A conservative interpretation is to associate 79-10, 79-13, 79-11 and 92-24 with a "young" age (roughly <12 ka) and 92-8 to an older age (roughly >12 ka).

6. Discussion

6.1. Volcanic architecture of the AVR

Our closely-spaced and re-navigated TOBI tracks have enabled us to produce a sidescan sonar mosaic of unprecedented precision; this, combined with the extensive ROV videos and ultra-high-resolution bathymetry from dives 87 and 91 has allowed us for the first time clearly to describe the nature and dimensions of the TOBI "hummocks". We can identify each hummock as a single volcano, dome to cone shaped, up to 450 m wide and 200 m high, and composed of pillows, lobate and elongated pillows. Other authors have referred to similar features as "pillow mounds" (Chadwick and Embley, 1994; Perfit and Chadwick, 1998; White et al., 2002). The AVR is almost entirely made up of such small volcanoes; it contains no smooth lava fields and only one flat-topped volcano, which may in fact be a lava terrace.

The hummocks are quite strongly grouped into volcanic lineaments, which can be observed in both the bathymetry and the sidescan data (insets, Figs. 1 and 2), and are referred to as "hummocky ridges" by Smith and Cann (1999). Most are chains of single hummocks. However, whereas Smith and Cann (1999) find that they extend predominantly along the summits of AVRs, we find they also occur on the AVR flanks (Figs. 1, 4 and 7). Some of these have higher magnetization than those along the AVR crest, implying the youngest volcanism may occur in the flanks. Many are oriented

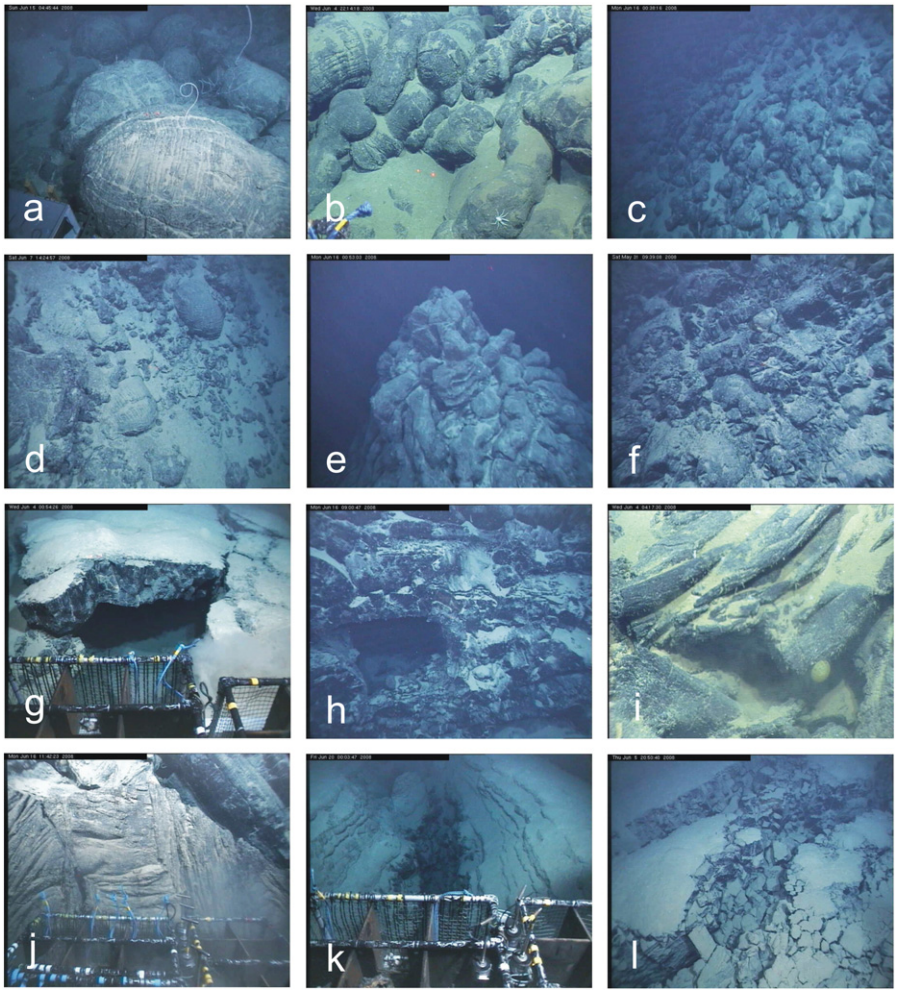

Fig. 6. Illustrative photographs from the *Isis* dives. Field of view is mostly about 2–4 m. a) Rounded pillow basalts (dive 88, 04 h:45 m:44 s GMT); b) slightly elongated pillows (dive 82, 22:14:18); c) steeply draped elongate pillows (dive 88, 00:38:16); d) pillow breccia (dive 85, 14:24:57); e) "haystack" on top of conical volcano (dive 88, 00:53:03); f) truncated pillows (dive 79, 09:39:08); g) sheet flow revealed in tumulus under flat-lying sediments (dive 81, 00:54:26); h) open lava tube revealed by fault scarp (dive 89, 09:00:47); i) pahoehoe (dive 81, 04:17:30); j) small dyke (dive 89, 11:42:31); k) approximately 1 m thickness of semi-indurated sediment revealed by fissuring west of the AVR (dive 92, 00:03:47); l) active fissuring on the median valley floor west of the AVR (dive 83, 20:50:40).

parallel to the AVR axis, and thus mark the expected trend of cracking, fissuring and dyking resulting from east–west spreading, and we interpret them as the results of linear, fissure-fed eruptions that evolved to a line of point-sources (Smith and Cann, 1999).

However, a number of the lineaments follow an oblique, northeast trend. We take this to reflect the slight regional obliquity of the spreading segments on this part of the MAR, which trend a few degrees anticlockwise from the regional ridge trend, and are accompanied by short dextral offsets (Keeton and Searle, 1996). Obliquely trending faults and volcanic lineaments are common in slow-spreading non-transform offsets (e.g., Grindlay et al., 1991; Searle and Laughton, 1977; Smith and Cann, 1999; Tyler et al., 2007) and are explained by rotation of stresses between the offset spreading segments (Grindlay and Fox, 1993; Tyler et al., 2007). Away from segment ends, curved and sigmoidal faults are seen with the same sense of offset (Lawson et al., 1996; Murton and Parson, 1993; Searle et al., 1998b), suggesting that an oblique shear stress can be present even away from non-transform offsets at segment ends.

In addition, many volcanic lineaments are normal to the AVR. These are hard to see on sidescan images whose insonification direction is AVR-normal (as in most surveys), and probably for this reason such features have not often been described. Smith and Cann (1999) do report that "close to segment centers" some hummocky ridges strike at a high angle to the AVR trend. While these appear to be similar to our orthogonal lineaments, we emphasise that at least at 45°N they are not confined to the segment centre (Fig. 7). Smith and Cann (1999) ascribe such "aberrant" trends to dyke injection controlled by high residual pressure in magma chambers situated near AVR centres, but this would not explain the occurrence of such features throughout the AVR, unless magma chambers also occur, possibly episodically, along its length. Unlike some volcanic lineaments studied in the MARK area (Bryan et al., 1994), the orthogonal lineaments do not appear to be controlled by prior topographic features. They do not follow expected tectonic trends, but are aligned down the steepest local gradients on the AVR flanks, suggesting their emplacement is gravity-controlled. Smith and Cann (1999) described lava terraces on the MAR at 29°–30°N and Puna Ridge (submarine flank of Kilauea, Hawaii) that cascade down the ~10°–15° flanks at right angles to the axes of those volcanic ridges, and which they state may even stand proud of the slope and form isolated small seamounts. They interpret these as secondary eruptive features, fed from tubes or channels sourced higher up the ridge flank or on its crest. Those lava terraces are much wider (~1 km) and flatter than the cones making up our orthogonal lineaments; we do not see similar features at 45°N, with the possible exception of the flat-topped feature at 45°34′N, 27°50′W. However, we suggest that a similar emplacement mechanism explains the down-slope alignment of our orthogonal ridges, with a line of volcanic hummocks being successively (or simultaneously) fed by lava tubes (we do not see evidence in our high-resolution bathymetry

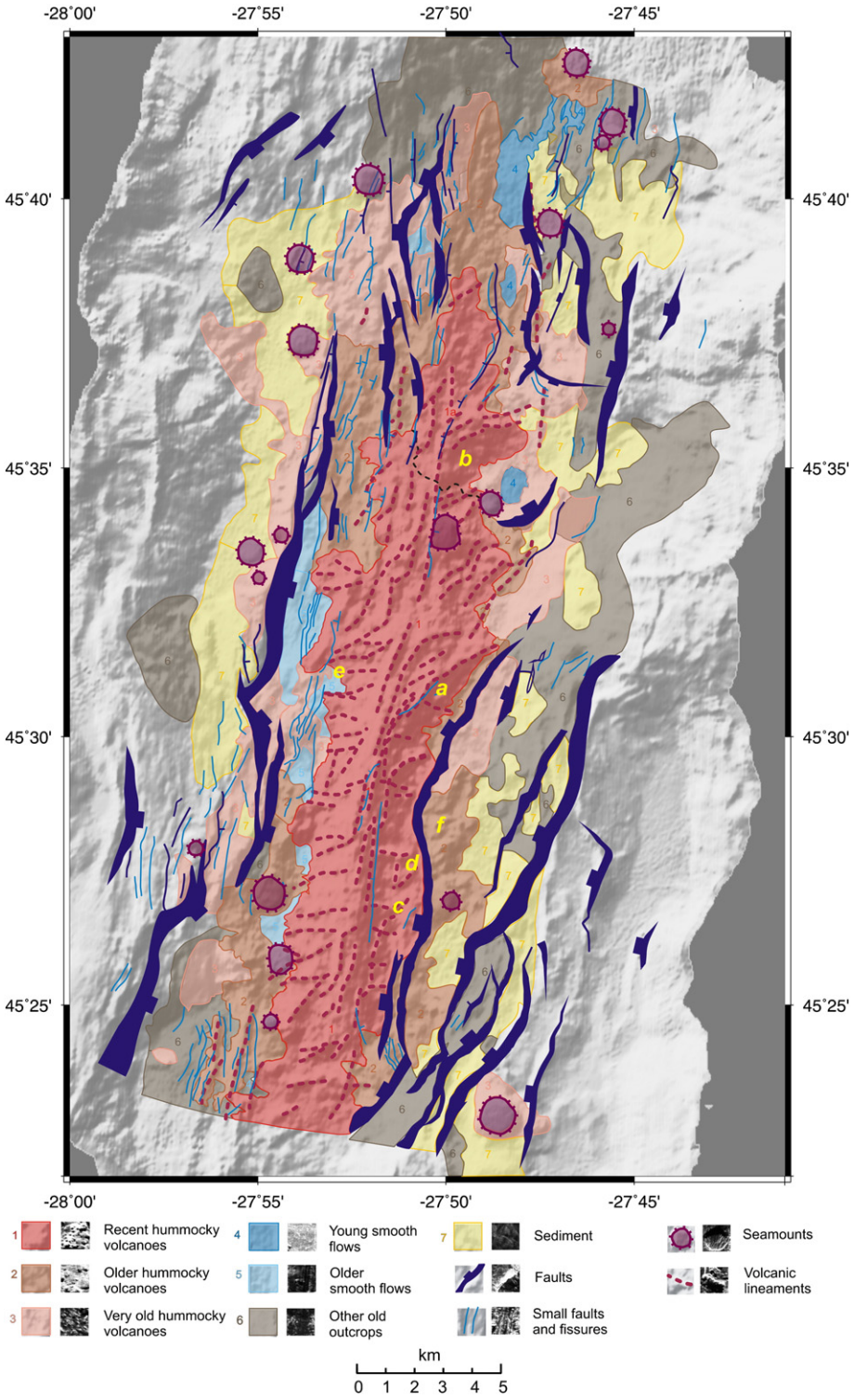

Fig. 7. Geological map derived primarily from TOBI sidescan data, draped over bathymetry illuminated from the NW. Sidescan images are often badly degraded during turns, so these areas have not been interpreted. Larger versions of the acoustic terrain panels in the key are shown in Figure 5. Yellow letters mark the same features identified in Figures 1 and 2 and discussed in the text.

for lava channels). Whether hummocks or terraces form probably depends on the available magma volume and extrusion rate.

Cann and Smith (2005) note that hummocks often cluster into larger volcanic mounds, within which they consider each hummock to be a single flow lobe of a larger pillow flow. We do recognise some "hummocky volcanoes", consisting of piles of individual hummocks, but we see no evidence that the cones are eruptive "lobes" of larger flows. Nevertheless, the spatial clustering, either into mounds or lineaments, does imply that all cones in a cluster are likely to share a single parental magma.

6.2. Smooth lava flows

The median valley surrounding the AVR is partly floored by smooth lava flows. Even those that have strong acoustic backscatter, which we interpret as relatively young, are mostly covered by a

Table 2
Preliminary palaeointensity results.

Sample	Longitude (degrees)	Latitude (degrees)	Distance from axis (km)	Spreading age (ka)	Inferred VADM (10^{22} A m$^{2)}$	Inferred minimum age (ka)	Inferred maximum age (ka)
79-3	−27.84050	45.48705	2.3	209	6.3	7	14
79-10	−27.84142	45.49467	2.0	182	11.3	1	9
79-11	−27.84387	45.49420	1.8	164	9.6	1	10
79-13	−27.84388	45.49415	1.8	164	10.8	1	9
92-8	−27.89735	45.48567	2.0	182	4.6	14	>25
92-24	−27.87675	45.48257	0.4	36	9.3	1	10
93-38	−27.86510	45.48495	0.5	45	21.5	–	–
Present field			0	0	10.8	0	0
B/M boundary			8.6	780			

veneer of sediment. The surface or interior of these lava flows is only rarely seen when it is exposed by faulting, fissuring, or in tumuli. True sheet flow textures such as pahoehoe are rare. Most lavas are flattened pillow lobes; occasional massive flows are exposed in valley-wall faults, but their flow textures cannot be determined. Cann and Smith (2005) found that the upper surfaces of flat-lying lava flows imaged by TOBI sidescan at MAR 25°N consisted entirely of pillows. We conclude that sidescan acoustic texture alone cannot be used to identify lava morphology, and especially sheet flows, though it probably can discriminate volcano morphology — i.e. presence or absence of hummocky volcanoes. The overall morphology of the smooth flows is very similar to the post-glacial lava flows on the Reykjanes Peninsula of Iceland, such as those produced by the Krisuvik Fires eruption of 1151 AD (e.g., Peate et al., 2009, and references therein). There is extensive evidence of growth by inflation, and of later lava draw-down leading to skylights and other collapse features. We sought extensively for the source of the young, flat lava field at the northern end of our survey; a possible location is the northernmost seamount in our survey area. This flow does not seem to extend as far as the northernmost high magnetization anomaly (which might have suggested it is very young). We cannot estimate the relative ages of the younger smooth flows and the AVR, which may be similar. The older smooth flows with their thick sediment cover must be older.

6.3. Faulting

We observe relatively little faulting, but some fissuring, on the main AVR, especially along its crest. We see a few minor faults in the AVR flanks, both inward and outward dipping, but they are rare. Some faults may have been buried by later volcanism and compose some of the observed volcanic lineaments. More faulting occurs on the older, northern part of the AVR, especially on its west flank where there are significant outward facing normal faults. This may be an early stage of AVR splitting, prior to rafting off-axis (Macdonald et al., 1975). Strong fissuring is observed in most of the median valley floor. Faults and

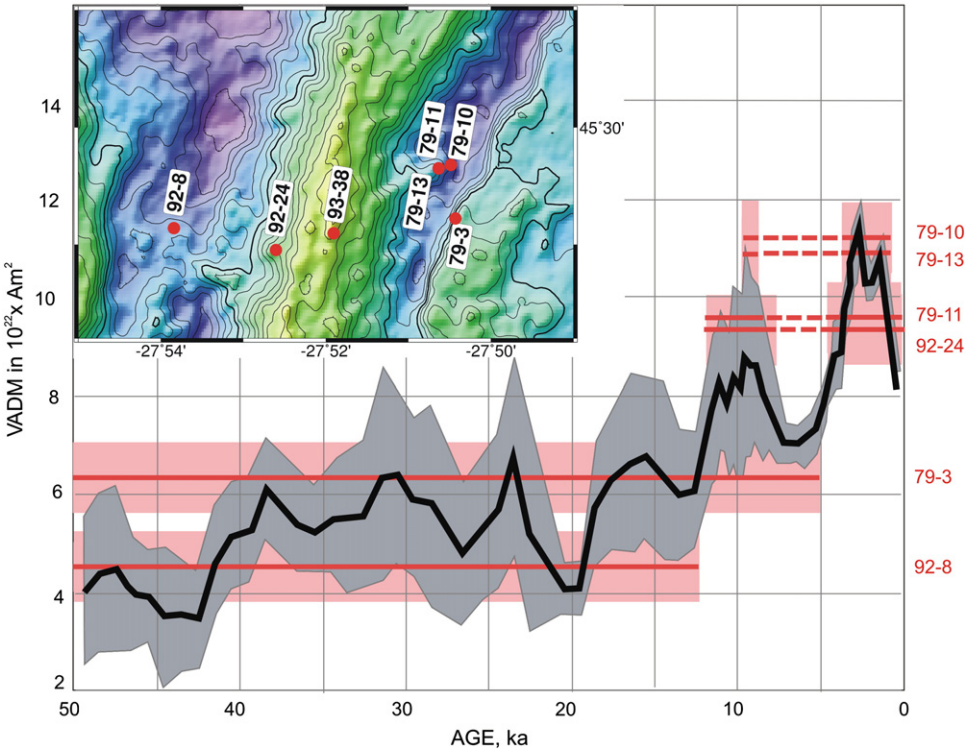

Fig. 8. Plot of magnetic palaeointensity expressed as Virtual Axial Dipole Moment (VADM) against time in thousands of years before present. Black line and grey shaded area: reconstructed variations in the geomagnetic dipole moment over the past 50 kyr from the GEOMAGIA50 database, redrawn from (Knudsen et al., 2008). Red numerals and horizontal lines indicate measured palaeointensities from this study. Experimental uncertainties (pink areas) of $\pm 0.7 \times 10^{22}$ A m^2 are estimated as twice the mean standard error from all individual units published by (Carlut et al., 2004) on the same kind of material. Age limits inferred from comparison with the reference curve are shown by solid red lines, with dashed lines indicating unlikely age ranges. Inset: bathymetry of the central part of the AVR and adjacent valley floor showing sample locations. Contour interval is 50 m with 3000 m in bold. See Section 5 for further discussion.

fissures are aligned either NNE (normal to the spreading direction) or NE, oblique in the sense expected for stress rotation at dextral ridge offsets.

This pattern of faulting and fissuring is similar to that seen at other slow-spreading segments on the MAR (Cann and Smith, 2005; Kong et al., 1988/89; Lawson et al., 1996; Searle et al., 1998a). In particular, there is a progressive development of tectonism from single fissures at the AVR crest, through minor normal faults on the AVR flanks, swarms of fissures and minor faults on the median valley floor, and increasing vertical offsets to develop major normal faults in the median valley walls. We do not observe a wide summit graben such as on the Snakepit AVR (Gente et al., 1991), but there is a small summit horst in places.

6.4. Age and development of AVR

We have attempted to estimate the ages of young seafloor via a number of proxies. The whole of our survey lies within the 17 km-wide Brunhes normal-polarity chron (780 ka; Cande and Kent, 1995; DeMets et al., 1994). The "spreading age" of the AVR, based on its 2 km half width and a half spreading rate of 11 km M yr^{-1} (DeMets et al., 1994), is 180 ka.

We have shown that sediment cover is a poor proxy for age within the range represented by the AVR, although there is a clear distinction between the tens of centimetres of cover on the AVR and young smooth flows and a metre or more cover on the older smooth flows. Given a sedimentation rate here of a few centimetres per thousand years (Keen and Manchester, 1970), this suggests ages of less than ~10 ka for the AVR, and greater than ~50 ka for the rest of the median valley floor.

Another potential proxy for age within the normal-polarity Brunhes is the strength of crustal magnetization (e.g., Allerton et al., 2000; Hussenoeder et al., 1996). The distance between the flanking magnetization minima is approximately 8 km (Fig. 3). This is typical of the ubiquitous "Central Anomaly Magnetic High" (Klitgord, 1976; Schouten et al., 1999, 2003; Tivey and Johnson, 1987). The CAMH is thought to reflect the approximately monotonic doubling of the strength of the Earth's field since about 40 ka (Gee et al., 2000; McElhinny and Senanayake, 1982). However, some processes not directly related to crustal age may also reduce magnetization, for example hydrothermal alteration or brecciation by faulting (Hussenoeder et al., 1996; Tivey and Johnson, 1987; Tivey et al., 1993). Moreover, our magnetization inversions assume a constant thickness magnetic source layer. If this varies, it could also cause variation in the inferred magnetization (Schouten et al., 1999). The correlation of high magnetization with the topographic ridges and cones (Fig. 4 and Supplementary Fig. 2) suggests this may be the case; we would then have a varying thickness magnetic source (presumably extrusive lavas), which itself would be evidence of a non-steady-state crustal accretion process. Even with these caveats, the narrowness of the CAMH suggests that the entire AVR is significantly younger than 780 ka, and probably less than 10 ka (Williams et al., 2008). This is consistent with the results of our palaeointensity measurements, which suggest age ranges of up to 12 ka for the AVR flanks and over 12 ka for the median valley floor.

Parson et al. (1993) presented a possible evolutionary scheme for AVR growth. The 45°N AVR appears to be in the "adolescent" phase in this scheme, having a high aspect ratio and consisting predominantly of thin, fissure-fed ridges with few large conical or flat-topped seamounts and relatively little faulting and sediment cover. Thirty well-defined AVRs on the MAR between 24°30′N and 30°30′N (Purdy et al., 1990) range from 4 to 36 km long, 1.5 to 8 km wide and 150 to 800 m high, so the 45°N AVR (18 km × 4 km × 500 m) lies firmly in the middle of this range. It is more fully developed than the young "Tadpole Ridge" at MAR 25°N, where the youngest hummocky flows are ~5 ka (Cann and Smith, 2005), but much less developed than the MARNOK AVR at MAR 24°35′N, which is interpreted to be up to ~20 ka in places (Lawson et al., 1996).

If our age estimates are correct, the volcanism on the 45°N AVR, and possibly parts of the surrounding median valley floor, are significantly younger than those predicted by a uniform age progression based on constant spreading rate. A similar conclusion was reached by Sturm et al. (2000) in the MARK area of the MAR. This may simply reflect a surficial spreading of magma beyond the range of a very narrow axial emplacement zone. However, as the AVR is composed almost entirely of individual volcanoes scattered more or less uniformly over it, such a distribution of magma would have to occur at depth, not via surficial flows as at the East Pacific Rise (Soule et al., 2007). Alternatively AVRs may not be entirely steady-state features, but reflect a degree of episodicity. Given that AVRs are almost ubiquitous along slow-spreading ridges, an age disparity as great as we infer between the AVR at 45°N and the "spreading age" of the crust on which it sits should be comparatively rare.

7. Conclusions

The most complete high resolution survey of an AVR to date has shown a coherent structure, formed almost entirely of small, steep volcanic cones or hummocks, whose precise nature we have demonstrated for the first time. Sediment cover is locally controlled by volcano topography, but overall volcanoes in the AVR appear to be of similar age. Many are rapidly degraded by flank collapse. They occasionally occur in clusters, but do not appear to be lobes of larger lava flows. They form prominent alignments, often following expected tectonic alignments, but including many that are normal to the AVR and occur along the whole AVR length. We propose these latter are fed from a common source with melt delivered down-slope under gravity, probably in lava tubes. These orthogonal alignments are significantly smaller than the stacked lava terraces reported from elsewhere on the MAR and Puna Ridge.

The AVR is partially surrounded by flat-lying lavas comprising smooth and lobate flows with evidence for subsurface supply channels, inflation and collapse. They have variable sediment cover, the youngest being roughly contemporaneous with the AVR volcanoes.

Flat-topped seamounts occur on the median valley floor but are rare on the AVR.

Tectonic strain begins with fissuring along the AVR crest, and develops progressively through sporadic fissures and small faults on the AVR flanks, through intense swarms of fissures and more frequent small faults on the median valley floor, to major, median-valley-wall faults. Few outward facing faults are exposed in the AVR flanks.

High acoustic backscatter suggests the AVR is relatively young. Crustal magnetization, taken as a proxy for age, is highest along the AVR crest and along some flanking volcanic lineaments. The width of the CAMH and provisional ages inferred from magnetic palaeointensity suggest the AVR is ~12 ka in age, flanked by ~120 ka crust; observed sediment thicknesses are consistent with this. This implies either episodic AVR development or redistribution of axially emplaced melt within or beneath the AVR. The AVR at 45°N appears to be at a mid-stage of development.

Supplementary materials related to this article can be found online at doi:10.1016/j.epsl.2010.09.003.

Acknowledgements

This work was funded by the Natural Environment Research Council as award NE/C520598/1 to Durham University and NE/C520612/1 to Southampton University. We gratefully acknowledge the professionalism and dedication of the officers, crew and shipboard technicians of James Cook cruise 24 in acquiring the data used here. Jean-Pierre Valet is thanked for allowing us to use his state-of-the-art

Palaeomagnetic Laboratory at l'Institut de Physique du Globe, Paris. We also acknowledge very helpful reviews by Dan Sauter, an anonymous reviewer, and the editor.

References

Allerton, S., Escartin, J., Searle, R.C., 2000. Extremely asymmetric magmatic accretion of oceanic crust at the ends of slow-spreading ridge-segments. Geology 28, 179–182.

Aumento, F., Loncarevic, B.D., Ross, D.I., 1971. Hudson Geotraverse: geology of the Mid-Atlantic Ridge at 45°N. Philos. Trans. R. Soc. London Ser. A 268, 623–650.

Ballard, R.D., Van Andel, T.H., 1977. Morphology and tectonics of the inner rift valley at lat. 36° 50′N on the Mid-Atlantic Ridge. Geol. Soc. Am. Bull. 88, 507–530.

Barclay, A.H., Toomey, D.R., Solomon, S.C., 1998. Seismic structure and crustal magmatism at the Mid-Atlantic Ridge, 35°N. J. Geophys. Res. 103 (B8), 17827–17844.

Bellaiche, G., Cheminee, J.L., Francheteau, J., Hekinian, R., Lepichon, X., Needham, H.D., Ballard, R.D., 1974. Inner floor of Rift Valley — first submersible study. Nature 250 (5467), 558–560.

Bideau, D., Hekinian, R., Sichler, B., Gracia, E., Bollinger, C., Constantin, M., Guivel, C., 1998. Contrasting volcanic–tectonic processes during the past 2 Ma on the Mid-Atlantic Ridge: submersible mapping, petrological and magnetic results at lat. 34°52′N and 33°55′ N. Mar. Geophys. Res. 20 (5), 425–458.

Blondel, P., Murton, B.J., 1997. Hand-book of Seafloor Sonar Imagery. Wiley and Sons, Chichester. 314 pp.

Bowles, J., Gee, J.S., Kent, D.V., Perfit, M.R., Soule, S.A., Fornari, D.J., 2006. Paleointensity applications to timing and extent of eruptive activity, 9 degrees–10 degrees N East Pacific Rise. Geochem. Geophys. Geosyst. 7.

Briais, A., Sloan, H., Parson, L., Murton, B., 2000. Accretionary processes in the axial valley of the Mid-Atlantic Ridge 27°–30°N from TOBI side-scan sonar images. Mar. Geophys. Res. 21, 87–119.

Brown, J.R., Karson, J.A., 1989. Variations in axial processes on the Mid-Atlantic Ridge: the median valley of the MARK area. Mar. Geophys. Res. 10, 109–138.

Bryan, W.B., Moore, J.G., 1977. Compositional variations of young basalts in the Mid-Atlantic rift valley near 36°49′N. Geol. Soc. Am. Bull. 88, 556–570.

Bryan, W.B., Humphris, S.E., Thompson, G., Casey, J.F., 1994. Comparative volcanology of small axial eruptive centers in the MARK area. J. Geophys. Res. 99, 2973–2984.

Cande, S., Kent, D., 1995. Revised calibration of the geomagnetic polarity timescale for the late Cretaceous and Cenozoic. J. Geophys. Res. 100 (B4), 6093–6095.

Cann, J.R., Smith, D.K., 2005. Evolution of volcanism and faulting in a segment of the Mid-Atlantic Ridge at 25 degrees N. Geochem. Geophys. Geosyst. 6.

Carlut, J., Kent, D.V., 2000. Paleointensity record in zero-age submarine basalt glasses: testing a new dating technique for recent MORBs. Earth Planet. Sci. Lett. 183 (3–4), 389–401.

Carlut, J., Cormier, M.-H., Kent, D.V., Donnelly, K.E., Langmuir, C.H., 2004. Timing of volcanism along the northern East Pacific Rise based on paleointensity experiments on basaltic glasses. J. Geophys. Res. 109 (B4) art. B04104.

Chadwick, W.W., Embley, R.W., 1994. Lava flows from a mid-1980s submarine eruption on the Cleft Segment, Juan-De-Fuca Ridge. J. Geophys. Res. Solid Earth 99 (B3), 4761–4776.

Coe, R.S., 1967. The determination of paleo-intensities of the Earth's magnetic field with emphasis on mechanisms which could cause non-ideal behavior in Thellier's method. J. Geomagn. Geoelec. 19, 157–179.

DeMets, C., Gordon, R.G., Argus, D.F., Stein, S., 1994. Effect of recent revisions to the geomagnetic reversal timescale on estimates of current plate motions. Geophys. Res. Lett. 21 (20), 2191–2194.

Flewellen, C., Millard, N., Rouse, I., 1993. TOBI, a vehicle for deep ocean survey. Electron. Commun. Eng. J. 85–93 (April 1993).

Gee, J.S., Cande, S.C., Hildebrand, J.A., Donelly, K., Parker, R.L., 2000. Geomagnetic intensity variations over the past 780 kyr obtained from near-seafloor magnetic anomalies. Nature 408, 827–832.

Gente, P., Auzende, J.M., Karson, J.A., Fouquet, Y., Mével, C., 1991. An example of a recent accretion on the Mid-Atlantic Ridge: the Snake Pit neovolcanic ridge (MARK area 23°22′N). Tectonophysics 190, 1–29.

German, C., Tyler, P., Griffiths, G., 2003. The maiden voyage of UK ROV “Isis”. Ocean Challenge 12 (3), 16–18.

Gracia, E., Parson, L., Bideau, D., Hekinian, R., 1998. Volcano–tectonic variability along segments of the Mid-Atlantic Ridge between Azores Platform and the Hayes Fracture zone: evidence from submersible and high resolution sidescan data. Spec. Publ. Geol. Soc. Lond. 148, 1–15.

Grindlay, N.R., Fox, P.J., 1993. Lithospheric stresses associated with non-transform offsets of the Mid-Atlantic Ridge — implications from a finite element analysis. Tectonics 12 (4), 982–1003.

Grindlay, N.R., Fox, P.J., Macdonald, K.C., 1991. Second-order ridge axis discontinuities in the South Atlantic: morphology, structure, and evolution. Mar. Geophys. Res. 13, 21–49.

Guspi, F., 1987. Frequency-domain reduction of potential field measurements to a horizontal plane. Geoexploration 24, 87–98.

Guyodo, Y., Richter, C., Valet, J.P., 1999. Paleointensity record from Pleistocene sediments (1.4–0 Ma) off the California Margin. J. Geophys. Res. Solid Earth 104 (B10), 22953–22964.

Head, J.W., Wilson, L., Smith, D.K., 1996. Mid-ocean ridge eruptive vent morphology and structure: evidence for dike widths, eruption rates, and evolution of eruptions and axial volcanic ridges. J. Geophys. Res. 101 (B12), 28,265–28,280.

Hussenoeder, S.A., Tivey, M.A., Schouten, H., Searle, R.C., 1996. Near-bottom magnetic survey of the Mid-Atlantic Ridge axis, 24°–24°40′N: implications for crustal accretion at slow spreading ridges. J. Geophys. Res. 101 (B10), 22,051–22,069.

Isezaki, N., 1986. A new shipboard three-component magnetometer. Geophysics 51 (10), 1992–1998.

Karson, J.A., Thompson, G., Humphris, S.E., Edmond, J.M., Bryan, W.B., Brown, J.R., Winters, A.T., Pockalny, R.A., Casey, J.R., C., C.A., Klinkhammer, G., Palmer, M.R., Kinzler, R.J., Sulanowska, M.M., 1987. Along-axis variations in seafloor spreading in the MARK area. Nature 328, 681–685.

Keen, M.J., Manchester, K.S., 1970. The Mid-Atlantic Ridge near 45°N. X. Sediment distribution and thickness from seismic reflection profiling. Can. J. Earth Sci. 7, 735–747.

Keeton, J.A., Searle, R.C., 1996. Analysis of Simrad EM12 multibeam bathymetry and acoustic backscatter data for seafloor mapping, exemplified at the Mid-Atlantic Ridge at 45° N. Mar. Geophys. Res. 18 (6), 663–688.

Klitgord, K.D., 1976. Sea-floor spreading: the central anomaly magnetisation high. Earth Planet. Sci. Lett. 29, 201–209.

Knudsen, M.F., Riisager, P., Donadini, F., Snowball, I., R., M., K., K., Pesonen, L.J., 2008. Variations in the geomagnetic dipole moment during the Holocene and the past 50 kyr. Earth Planet. Sci. Lett. 272, 319–329.

Kong, L.S., Detrick, R.S., Fox, P.J., Mayer, L.A., Ryan, W.B.F., 1988/89. The morphology and tectonics of the MARK area from Sea Beam and Sea MARC I observations (Mid-Atlantic Ridge 23°N). Mar. Geophys. Res. 10, 59–90.

Korenaga, J., 1995. Comprehensive analysis of marine magnetic vector anomalies. J. Geophys. Res. 100 (B1), 365–378.

Lawson, K., Searle, R.C., Pearce, J.A., Browning, P., Kempton, P., 1996. Detailed volcanic geology of the MARNOK area, Mid-Atlantic Ridge north of Kane transform, tectonic, magmatic, hydrothermal and biological segmentation of mid-ocean ridges. Geol. Soc. Lond. Spec. Publ. 118, 61–102.

Macdonald, K., Luyendyk, B.P., Mudie, J.D., Spiess, F.N., 1975. Near-bottom geophysical study of Mid-Atlantic Ridge median valley near lat 37 degrees N — preliminary observations. Geology 3 (4), 211–215.

Macdonald, K.C., Fox, P.J., Alexander, R.T., Pockalny, R., Gente, P., 1996. Volcanic growth faults and the origin of pacific abyssal hills. Nature 380 (6570), 125–129.

McElhinny, M.W., Senanayake, W.E., 1982. Variations in the geomagnetic dipole 1. The past 50,000 years. J. Geomagn. Geoelec. 34, 39–51.

Mejia, V., Opdyke, N.D., Perfit, M.R., 1996. Paleomagnetic field intensity recorded in submarine basaltic glass from the East Pacific Rise, the last 69 kA. Geophys. Res. Lett. 23 (5), 475–478.

Mello, S.L.M., Cann, J.R., Fowler, C.M.R., 1999. Anomalous mantle at 45 degrees N Mid-Atlantic Ridge? J. Geophys. Res. Solid Earth 104 (B12), 29335–29349.

Mendel, V., Sauter, D., Rommevau-Jestin, C., Patriat, P., Levebvre, F., Parson, L.M., 2003. Magmato-tectonic cyclicity at the ultra-slow spreading Southwest Indian Ridge: evidence from variations of axial volcanic ridge morphology and abyssal hills pattern. Geochem. Geophys. Geosyst. 4 (5), 9102. doi:10.1029/2002GC000417.

Murton, B.J., Parson, L.M., 1993. Segmentation, volcanism and deformation of oblique spreading centres: a quantitative study of the Reykjanes Ridge. Tectonophysics 222, 237–257.

Parker, R.L., Huestis, S.P., 1974. The inversion of magnetic anomalies in the presence of topography. J. Geophys. Res. 79, 1587–1593.

Parson, L.M., Murton, B.J., Searle, R.C., Booth, D., Evans, J., Field, P., Keeton, J., Laughton, A., McAllister, E., Millard, N., Redbourne, L., Rouse, I., Shor, A., Smith, D., Spencer, S., Summerhayes, C., Walker, C., 1993. En echelon volcanic ridges at the Reykjanes Ridge: a life cycle of volcanism and tectonics. Earth Planet. Sci. Lett. 117, 73–87.

Peate, D.W., Baker, J.A., Jakobsson, S.P., Waight, T.E., Ken, A.J.R., Grassineau, N.V., Skovgaard, A.C., 2009. Historic magmatism on the Reykjanes Peninsula, Iceland: a snap-shot of melt generation at a ridge segment. Contrib. Mineralog. Petrol. 157 (3), 359–382.

Perfit, M.R., Chadwick, W.W., 1998. Magmatism at Mid-Ocean Ridges: constraints from volcanological and geochemical investigations. Faulting and Magmatism at Mid-Ocean Ridges. Geophysical Monograph, 106. American Geophysical Union, Washington, D.C., pp. 59–115.

Pick, T., Tauxe, L., 1993. Holocene paleointensities — Thellier experiments on submarine basaltic glass from the East Pacific Rise. J. Geophys. Res. Solid Earth 98 (B10), 17949–17964.

Purdy, G.M., Sempere, J.-C., Schouten, H., DuBois, D.L., Goldsmith, R., 1990. Bathymetry of the Mid-Atlantic Ridge, 24°–31°N: a map series. Mar. Geophys. Res. 12, 247–252.

Sauter, D., Parson, L., Mendel, V., Rommevaux-Jestin, C., Gomez, O., Briais, A., Mevel, C., Tamaki, K., the FUJI Scientific Team, 2002. TOBI sidescan sonar imagery of the very slow-spreading Southwest Indian Ridge: evidence for along-axis magma distribution. Earth Planet. Sci. Lett. 199 (1–2), 81–95.

Schouten, H., Tivey, M.A., Fornari, D.J., Cochran, J.R., 1999. Central anomaly magnetization high: constraints on the volcanic construction and architecture of seismic layer 2A at a fast-spreading mid-ocean ridge, the EPR at 9°30′–50′N. Earth Planet. Sci. Lett. 169, 37–50.

Schouten, H., Tivey, M., Fornari, D., Yoerger, D., Bradley, A., Edwards, M., Johnson, P., 2003. Central anomaly magnetization high: constraints on the volcanic construction and architecture of young upper oceanic crust, EPR 9°–10°N, Ridge 2000 Events (April), pp. 30–34.

Searle, R.C., Bralee, A.V., 2007. Asymmetric generation of oceanic crust at the ultra slow spreading Southwest Indian Ridge, 64ºE. Geochem. Geophys. Geosyst. 8 (5), Q05015. doi:10.1029/2006GC001529.

Searle, R.C., Laughton, A.S., 1977. Sonar studies of the Mid-Atlantic Ridge crest near Kurchatov Fracture Zone. J. Geophys. Res. 82, 5313–5328.

Searle, R.C., Cowie, P.A., Mitchell, N.C., Allerton, S., MacLeod, C.J., Escartin, J., Russell, S.M., Slootweg, P.A., Tanaka, T., 1998a. Fault structure and detailed evolution of a slow spreading ridge segment: the Mid-Atlantic Ridge at 29°N. Earth Planet. Sci. Lett. 154 (1–4), 167–183.

Searle, R.C., Keeton, J.A., Lee, S.M., Owens, R., Mecklenburgh, R., Parsons, B., White, R.S., 1998b. The Reykjanes Ridge: structure and tectonics of a hot-spot influenced, slow-

spreading ridge, from multibeam bathymetric, gravity and magnetic investigations. Earth Planet. Sci. Lett. 160, 463–478.
Sempéré, J.-C., Purdy, G.M., Schouten, H., 1990. Segmentation of the Mid-Atlantic Ridge between 24°N and 30°40′N. Nature 344, 427–431.
Sinha, M.C., Constable, S.C., Peirce, C., White, A., Heinson, G., MacGregor, L.M., Navin, D.A., 1998. Magmatic processes at slow-spreading ridges: implications of the RAMESSES experiment at 57°45′N on the Mid-Atlantic Ridge. Geophys. J. Int. 135 (3), 731–745.
Smith, D.K., Cann, J.R., 1992. The role of seamount volcanism in crustal construction at the Mid-Atlantic Ridge (24°–30°N). J. Geophys. Res. 97, 1645–1658.
Smith, D.K., Cann, J.R., 1999. Constructing the upper crust of the Mid-Atlantic Ridge: a reinterpretation based on Puna Ridge, Kilauea Volcano. J. Geophys. Res. B 104 (25), 379–25399.
Smith, D.K., Cann, J.R., Dougherty, M.E., Lin, J., Spencer, S., MacLeod, C., Keeton, J., McAllister, E., Borroks, B., Pascoe, R., Robertson, W., 1995. Mid-Atlantic Ridge volcanism from deep-towed side-scan sonar images, 25°–29°N. J. Volcanol. Geoth. Res. 67 (4), 233–262.
Soule, S.A., Fornari, D.J., Perfit, M.R., Rubin, K.H., 2007. New insights into mid-ocean ridge volcanic processes from the 2005–2006 eruption of the East Pacific Rise, 9 degrees 46′ N–9 degrees 56′ N. Geology 35 (12), 1079–1082.
Sturm, M., Goldstein, S., Klein, E.M., Karson, J.A., Murrell, M.T., 2000. Uranium-series age constraints on lavas from the axial valley of the Mid-Atlantic Ridge, MARK area. Earth Planet. Sci. Lett. 181, 61–70.
Thatcher, W., Hill, D.P., 1995. A simple model for the fault-generated morphology of slow-spreading mid-oceanic ridges. J. Geophys. Res. 100 (B1), 561–570.
Thellier, E., Thellier, O., 1959. Sur l'intensité du champ magnétique terrestre dans le passé historique et géologique. Ann. Geophys. 15, 285–378.
Tivey, M.A., Johnson, H.P., 1987. The central anomaly magnetic high: implications for ocean crust construction and evolution. J. Geophys. Res. 92, 12,685–12,694.
Tivey, M.A., Rona, P.A., Schouten, H., 1993. Reduced crustal magnetization beneath the active sulfide mound, TAG hydrothermal field, Mid-Atlantic Ridge at 26°N. Earth Planet. Sci. Lett. 115, 101–115.
Tyler, S., Bull, J.M., Parson, L.M., Tuckwell, G.W., 2007. Numerical modelling of non-transform discontinuity geometry: implications for ridge structure, volcano–tectonic fabric development and hydrothermal activity at segment ends. Earth Planet. Sci. Lett. 257 (1–2), 146–159.
Wessel, P., Smith, W.H.F., 1998. The Generic Mapping Tools (GMT) version 3.4 Technical Reference and Cookbook, SOEST/NOAA.
White, S.M., Macdonald, K.C., Sinton, J.M., 2002. Volcanic mound fields on the East Pacific Rise, 16 degrees–19 degrees S: low effusion rate eruptions at overlapping spreading centers for the past 1 Myr. J. Geophys. Res. Solid Earth 107 (B10) art. no.-2240.
Williams, C.M., Tivey, M.A., Schouten, H., Fornari, D.J., 2008. Central anomaly magnetization high documentation of crustal accretion along the East Pacific Rise (9° 55′–9° 25′ N). Geochem. Geophys. Geosyst. 9.
Yeo, I., Searle, R.C., Achenbach, K., LeBas, T. and JC07 Shipboard Scientific Party, under revision. Small, discrete volcanoes: building blocks of the upper oceanic crust. Geology.